

See discussions, stats, and author profiles for this publication at: <https://www.researchgate.net/publication/270582648>

New Members of the Family of In-Sb-S Compounds: Different Roles of Organic Amines

ARTICLE *in* CRYSTAL GROWTH & DESIGN · NOVEMBER 2014

Impact Factor: 4.89 · DOI: [10.1021/cg5015779](https://doi.org/10.1021/cg5015779)

CITATION

1

READS

10

8 AUTHORS, INCLUDING:



Kai-Yao Wang

Jacobs University

13 PUBLICATIONS 70 CITATIONS

[SEE PROFILE](#)



du cf

Chinese Academy of Sciences

13 PUBLICATIONS 40 CITATIONS

[SEE PROFILE](#)



Mei-Ling Feng

Chinese Academy of Sciences

60 PUBLICATIONS 510 CITATIONS

[SEE PROFILE](#)



Xiao-Ying Huang

Chinese Academy of Sciences

330 PUBLICATIONS 6,037 CITATIONS

[SEE PROFILE](#)

New Members of the Family of In–Sb–S Compounds: Different Roles of Organic Amines

Kai-Yao Wang,[†] Bo Zhang,^{†,‡} Xing-Hui Qi,^{†,§} Nan-Nan Shen,^{†,‡} Cheng-Feng Du,^{†,‡} Zhao-Feng Wu,^{†,‡} Mei-Ling Feng,[†] and Xiao-Ying Huang^{*,†}

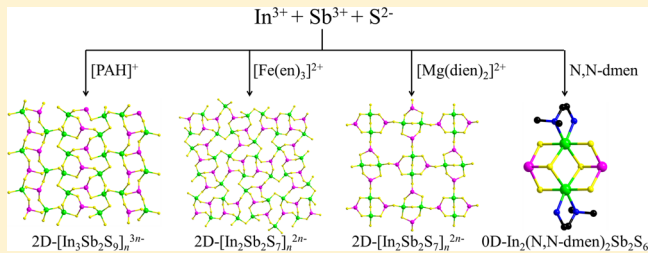
[†]State Key Laboratory of Structural Chemistry, Fujian Institute of Research on the Structure of Matter, Chinese Academy of Sciences, Fuzhou, Fujian 350002, P. R. China

[‡]University of Chinese Academy of Sciences, Beijing, 100049, P. R. China

[§]College of Chemistry, Fuzhou University, Fuzhou, Fujian 350002, P.R. China

S Supporting Information

ABSTRACT: Reported here are the syntheses, structures, and characterizations of four novel In–Sb–S compounds containing organic amines, namely, $[PAH]_3[In_3Sb_2S_9]$ ($PA = n$ -propylamine) (1), $[Fe(en)]_3[In_2Sb_2S_7]$ ($en = ethylenediamine$) (2), $[Mg(dien)]_2[In_2Sb_2S_7] \cdot 0.5H_2O$ ($dien = diethylenetriamine$) (3), and $In_2(N,N-dmen)_2Sb_2S_6$ ($N,N-dmen = N,N$ -dimethylethylenediamine) (4). Compound 1 features a $[In_3Sb_2S_9]_{3n}^{2n-}$ layer assembled by the alternating linkage of the $\{In_2Sb_2S_8\}_n$ ribbons and the $\{In_4Sb_2S_{12}\}_n$ double-ribbons. Both compounds 2 and 3 possess layered anionic parts with the same stoichiometry of $[In_2Sb_2S_7]_{2n}^{2n-}$ but distinct linkage modes between the subunits of $\{In_2S_7\}$ groups and Sb^{3+} ions. Notably, the $\{In_2Sb_2S_9\}$ heterometallic cluster observed in 3 is initially regarded as the secondary building unit (SBU) for the construction of the $[In_2Sb_2S_7]_{2n}^{2n-}$ layer. Compound 4 features a novel discrete inorganic–organic hybrid molecule of $In_2(N,N-dmen)_2Sb_2S_6$. Through the structural analyses on 1–4, the organic amines applied played three different roles on the formation of the final crystalline products. For 1, the protonated n -propylamines arrange in the space around the anionic network and balance the negative charge. For 2 and 3, the chelating polyamines coordinate to central metal ions to form metal complexes, which then act as space-filling and charge-balancing agents. For 4, two N,N -dimethylethylenediamines chelate to two In^{3+} ions of the inorganic segment through coordination bonds, leading to the formation of a rare inorganic–organic hybrid cluster. At last, we gave a systematic discussion about the characteristics and roles of organic amines in all related In–Sb–S compounds. In one word, the work presented here enriches the structural chemistry of the main-group heterometallic chalcogenidometalates, providing more chances for researchers to work out the rules in their composition– or structure–function relationship.



INTRODUCTION

From the early work by Bedard et al. in 1989, the solvothermal synthesis of main-group chalcogenidometalates applying amines has caught lots of attention.^{1–6} As for binary chalcogenidoantimonate Sb_xQ_y ($Q = S, Se, Te$) moieties, their large structural diversity has made them excellent candidates to integrate other metal ions to build ternary phases. In the past two decades, successful work has been done on the integration of transition metal (TM) ions into the Sb_xQ_y moieties to form TM–Sb–Q (TM = Cr,^{7–10} Mn,^{11–18} Fe,^{19,20} Co,^{21–25} Ni,^{23,26} Zn,^{26,27} Cu,^{28–34} and Ag^{35–41}) compounds. More recently, the increasing interest in main-group heterometallic M–Sb–Q (M = Ga, In, Ge, Sn) compounds stems from not only the construction of novel structural types that combine varied {MS_x} polyhedra but also their unique overall topologic categories.⁴² Among them, the studies on In–Sb–S compounds represent a relatively well-established research area, evidenced by different compositions of these compounds as well as their diverse structural features ranging from discrete

species to one-, two-, or three-dimensional architectures. Recent physical property studies on this family of compounds illustrated that some excellent performances such as selective ion-exchange and photocatalysis were strongly related to their specific compositions and structures.^{43,44} In turn, the further improvement of the composition– or structure–function relationships stimulates us all the time to develop the synthetic and structural chemistry of these materials.

Herein, we report on four novel In–Sb–S compounds prepared in different solvothermal conditions, namely, $[PAH]_3[In_3Sb_2S_9]$ (1), $[Fe(en)]_3[In_2Sb_2S_7]$ (2), $[Mg(dien)]_2[In_2Sb_2S_7] \cdot 0.5H_2O$ (3), and $In_2(N,N-dmen)_2Sb_2S_6$ (4). From the viewpoint of coordination chemistry, the organic amines in 1–4 played three different roles which contributed their distinct final solid-state structures to a great extent. These roles

Received: November 17, 2013

Revised: November 11, 2014



Table 1. Summary of Crystal Data for Compounds 1–4

	1	2	3	4
empirical formula	C ₉ H ₃₀ In ₃ N ₃ S ₉ Sb ₂	C ₆ H ₂₄ FeIn ₂ N ₆ S ₇ Sb ₂	C ₈ H ₂₇ In ₂ MgN ₆ O _{0.5} S ₇ Sb ₂	C ₈ H ₂₄ In ₂ N ₄ S ₆ Sb ₂
formula wt	1056.86	933.72	937.23	841.81
cryst syst	monoclinic	monoclinic	orthorhombic	monoclinic
space group	P2 ₁ /n	P2 ₁ /n	Aba2	P2 ₁ /c
T/K	296(2)	293(2)	293(2)	293(2)
$\lambda/\text{\AA}$	0.71073	0.71073	0.71073	0.71073
$a/\text{\AA}$	12.4629(6)	11.2266(4)	17.4725(8)	9.1428(12)
$b/\text{\AA}$	7.1421(3)	17.1624(6)	17.4610(7)	9.5960(13)
$c/\text{\AA}$	34.2641(14)	13.2954(5)	18.0777(9)	13.115(2)
α/deg	90	90	90	90
β/deg	96.458(4)	112.798(4)	90	102.290(14)
γ/deg	90	90	90	90
$V/\text{\AA}^3$	3030.5(2)	2361.57(15)	5515.3(4)	1124.3(3)
Z	4	4	8	2
$D_c/\text{Mg}\cdot\text{m}^{-3}$	2.316	2.626	2.257	2.487
μ/mm^{-1}	4.633	5.406	4.153	4.959
$F(000)$	1992	1760	3560	792
measd reflns	11365	10978	7921	4900
indep reflns	5328	5105	4122	2119
R_{int}	0.0347	0.0342	0.0238	0.0376
no. of params	305	236	245	102
GOF	1.044	1.008	1.008	1.000
Flack param			-0.01(5)	
R1, ^a wR2 [$I > 2\sigma(I)$]	0.0716, 0.1686	0.0314, 0.0594	0.0359, 0.1139	0.0388, 0.0716
R1, wR2 (all data)	0.0905, 0.1792	0.0473, 0.0653	0.0427, 0.1251	0.0592, 0.0792

$$^a \text{R1} = \sum ||F_o| - |F_c|| / \sum |F_o|, \text{wR2} = \{ \sum w[(F_o)^2 - (F_c)^2]^2 / \sum w[(F_o)^2]^2 \}^{1/2}.$$

are summarized as follows: (a) The protonated organic amines fill in the space around the inorganic framework, balancing the negative charge and interacting with the framework by van der Waals forces and hydrogen bonding. (b) The chelating polyamines (L) combine with central metal ions to form metal complexes [ML_m]ⁿ⁺, which play roles similar to that of protonated organic amines. (c) The amines interact with the Mⁿ⁺ ions of inorganic segments through coordination bonds to form inorganic–organic hybrids. Furthermore, systematic comparisons among all the In–Sb–S architectures directed by amine-involved species are given in this paper, revealing some primary relationships between the characteristics of organic species and their corresponding inorganic structures.

EXPERIMENTAL SECTION

Materials and Methods. All the analytical grade chemicals employed in this study were commercially available and used without further purification. Elemental analyses (C, H, and N) were performed using a German Elementary Vario EL III instrument. Energy-dispersive X-ray spectroscopy (EDS) was recorded on a JEOL JSM-6700F scanning electron microscope. The solid-state UV/vis spectra were measured at room temperature using a UV–vis–NIR Varian Cary 500 Scan spectrophotometer (for **1**, **2**, and **4**) and a PE Lambda 900 UV/vis spectrophotometer (for **3**), and a BaSO₄ plate was used as a standard (100% reflectance). The absorption (α/S) data were calculated from reflectance spectra by using the Kubelka–Munk function: $\alpha/S = (1 - R)^2/2R$,⁴⁵ where α is the absorption coefficient, S is the scattering coefficient which is practically independent of wavelength when the particle size is larger than 5 μm , and R is the reflectance. Powder X-ray diffraction (PXRD) patterns were recorded in the angular range of $2\theta = 5\text{--}65^\circ$ on a Miniflex II diffractometer using Cu K α radiation.

Syntheses of Compounds 1–4. [PAH]₃[In₃Sb₂S₉] (**1**). A mixture of In₂S₃ (0.244 g, 0.75 mmol), Sb₂S₃ (0.170 g, 0.5 mmol), S (0.08 g, 2.5 mmol), *n*-propylamine (1.5 mL), and ethanol (4 mL) was sealed in

a stainless steel reactor with a 20 mL Teflon liner and heated at 160 °C for 10 days. Then the closed apparatus was taken out from the oven and cooled to room temperature naturally under ambient conditions. The product was washed by distilled water and ethanol and then dried in the air. Tiny pale-yellow platelike crystals of **1** could be obtained in the yield of 0.309 g, 59% based on In. Anal. Calcd for C₉H₃₀In₃N₃S₉Sb₂: C, 10.23%; H, 2.86%; N, 3.98%. Found: C, 9.90%; H, 2.83%; N, 3.82%.

[Fe(en)₃]₂[In₂Sb₂S₇] (**2**). A mixture of In(0.057 g, 0.5 mmol), Sb (0.061 g, 0.5 mmol), Fe (0.0168 g, 0.3 mmol), S (0.064 g, 2 mmol), ethylenediamine (2.5 mL), and H₂O (0.5 mL) was sealed in a stainless steel reactor with a 28 mL Teflon liner and heated at 190 °C for 7 days. Then the closed apparatus was taken out from the oven and cooled to room temperature naturally under ambient conditions. The product was washed by distilled water and ethanol and then dried in the air. Dark yellow block crystals of **2** could be obtained in the yield of 0.133 g, 57% based on In. Anal. Calcd for In₂S₂Sb₂C₆H₂₄FeN₆: C, 7.72%; H, 2.59%; N, 9.00%. Found: C, 7.42%; H, 2.48%; N, 8.72%.

[Mg(dien)₂]₂[In₂Sb₂S₇]·0.5H₂O (**3**). A mixture of In(NO₃)₃·5H₂O (0.548 g, 1.4 mmol), Sb₂S₃ (0.238 g, 0.7 mmol), S (0.106 g, 3.3 mmol), MgCl₂·6H₂O (0.142 g, 0.7 mmol), and diethylenetriamine (5 mL) was sealed in a stainless steel reactor with a 20 mL Teflon liner and heated at 190 °C for 5 days. Then the closed apparatus was taken out from the oven and cooled to room temperature naturally under ambient conditions. The product was washed by distilled water and ethanol and then dried in the air. Pale-yellow platelike crystals of **3** could be obtained in the yield of 0.385 g, 58.6% based on In. Anal. Calcd for C₈H₂₇In₂MgN₆O_{0.5}S₇Sb₂: C, 10.25%; H, 2.90%; N, 8.97%. Found: C, 10.83%; H, 3.07%; N, 9.90%.

In₂(N,N-dmen)₂Sb₂S₆ (**4**). A mixture of In(NO₃)₃·5H₂O (0.196 g, 0.5 mmol), SbCl₃ (0.114 g, 0.5 mmol), thiourea (0.230 g, 3.00 mmol), and *N,N*-dimethylethylenediamine (8 mL) was sealed in a stainless steel reactor with a 20 mL Teflon liner and heated at 160 °C for 5 days. Then the closed apparatus was taken out from the oven and cooled to room temperature naturally under ambient conditions. The product was washed by distilled water and ethanol and then dried in the air. Pale-yellow block crystals of **4** could be obtained in the yield of

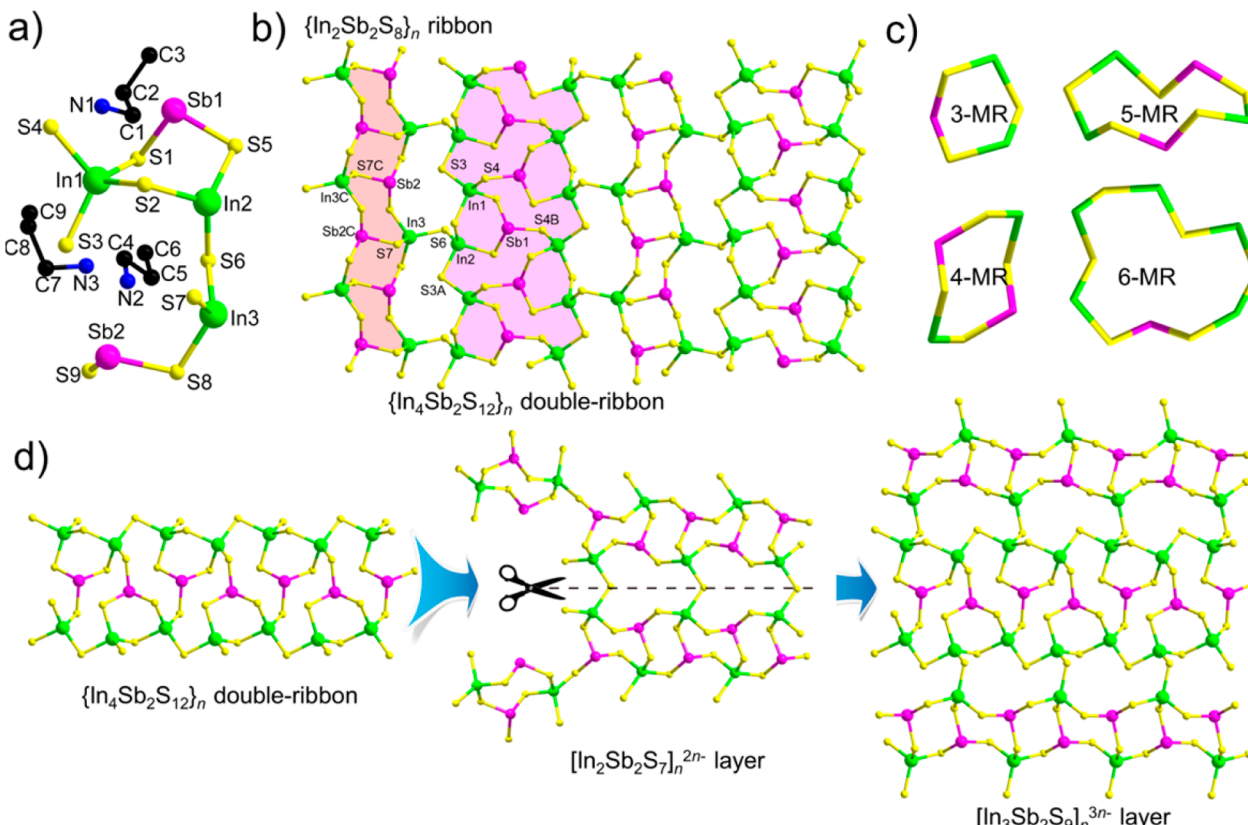


Figure 1. Ball-and-stick representations of (a) the asymmetric unit in **1** and (b) the structure of the $[In_3Sb_2S_9]_{n}^{3n-}$ layer constructed by the linkage of $\{In_4Sb_2S_{12}\}_n$ and $\{In_2Sb_2S_8\}_n$ ribbons. (c) Wire/stick representations of the 3-MR of $\{In_2SbS_3\}$, 4-MR of $\{In_2Sb_2S_8\}$, 5-MR of $\{In_3Sb_2S_5\}$, and 6-MR of $\{In_5Sb_6S\}$ in the layer of **1**. (d) Representation of the formation of the $[In_3Sb_2S_9]_{n}^{3n-}$ layer through the reassembly of the $[In_2Sb_2S_7]_{n}^{2n-}$ layer by incorporating the $\{In_4Sb_2S_{12}\}_n$ double-ribbon. H atoms and disordered C and N atoms are omitted for clarity. Symmetry codes: A ($x, -1 + y, -z$); B ($0.5 - x, -0.5 + y, 0.5 - z$); C ($1 - x, 1 - y, -z$).

0.018 g, 9% based on In. Anal. Calcd for $C_8H_{24}In_2N_4S_6Sb_2$; C, 11.41%; H, 2.87%; N, 6.66%. Found: C, 11.45%; H, 2.93%; N, 6.64%.

Single-Crystal Structure Determination. Single-crystal X-ray diffraction data of **1–4** were collected on an Xcalibur E Oxford diffractometer with graphite monochromatized Mo K α radiation ($\lambda = 0.71073 \text{ \AA}$) at room temperature. The absorption corrections were applied using multiscan technique. The structures of the four compounds were solved by direct methods and refined by full-matrix least-squares on F^2 using the SHELXL-97 program.⁴⁶ Non-hydrogen atoms were refined with anisotropic displacement parameters, and the hydrogen atoms bonded to C and N atoms were positioned with idealized geometry. The empirical formulas were confirmed by thermogravimetric analyses (TGA) and elemental analyses (EA) results. The relevant crystallographic data and structure refinement details are listed in Table 1, and the selected hydrogen bonding data of **1–4** are given in Table S1 in the Supporting Information.

RESULTS AND DISCUSSION

Syntheses of **1–4.** For the preparation of chalcogenido-metals, the solvothermal method has proven to be an effective technique, which can be significantly affected by initial reactants, pressure, reaction time, temperature, pH value, solvent, and so on. This synthetic approach was widely developed in the last two decades by applying organic amine species as medium, some of which possess appropriate boiling point and viscosity for the general solvothermal synthesis at relatively low temperature (100–200 °C) and low pressure, such as dipropylamine and ethylenediamine. Remarkable progress has been made by several research groups on the syntheses of chalcogenidoantimonates by using this method.

Recently, we further developed it in the syntheses of main-group heterometallic M–Sb–S compounds by replacing organic amines as *N,N*-dimethylformamide (DMF).^{43,47,48} Under solvothermal conditions, the reactions provide *in situ* formed $[(Me)_2NH_2]^+$ cation due to the hydrolysis of DMF, filling in the space around inorganic framework and balancing its negative charges.

Moreover, one of our latest research interests is to solvothermally prepare main-group heterometallic chalcogenidoantimonates by using mixed amine and ethanol as solvent. By using this method, we recently synthesized the first protonated methylamine-containing 13/15/16 group compound $[NH_3CH_{3}]_4[In_4SbS_3SH]$.⁴⁴ The high Rb $^+$ absorption capacity of this compound demonstrated a significant role of the pore size of the framework on the ion-exchange selectivity. Here, we prepared the new compound **1** through the similar reaction of In₂S₃ and Sb₂S₃ in stoichiometric ratio and excessive S powder, nevertheless applying *n*-propylamine instead of methylamine. By contrast, replacement of starting materials as elemental In, Sb, and S did not give any ideal result. Moreover, it is worth noting that the synthetic procedure was systematically optimized by adjusting two vital parameters, namely, the *n*-propylamine/ethanol volumetric ratios (from 1:20 to 1:2) and reaction time (from 5 days to 10 days), the optimums of which came out to be 7.5:20 and 10 days, respectively.

Compounds **2–4** were all synthesized by using chelating polyamines as solvents, nevertheless the reactants as well as the types of polyamines were widely distinct. For the preparation of

compound **2**, the elemental In, Sb, Fe, and S underwent a redox reaction that transferred their oxidation states to +3, +3, +2, and -2, respectively. This typical procedure is well-established and proves to be effective in the synthetic chemistry of group 13, 14, and 15 metallic chalcogenidometalates according to the literature.⁶ However, this strategy did not work in the preparation of compounds **3** and **4**, which were obtained by applying $\text{In}(\text{NO}_3)_3 \cdot 5\text{H}_2\text{O}$ and Sb_2S_3 (or SbCl_3) as the In^{3+} and Sb^{3+} sources, respectively. Especially in **4**, the thiourea supplied the S^{2-} in the final product, through a decomposition process upon heating or due to other influencing factors, comparable to some similar transformations in the literature.^{49,50} Clearly, the low oxidizability of thiourea compared to elemental S makes the In^{3+} and Sb^{3+} salts reasonable reagents here.

Description of Crystal Structures of 1–4. $[\text{PAH}]_3[\text{In}_3\text{Sb}_2\text{S}_9]$ (**1**). Compound **1** crystallizes in the space group $P2_1/n$, featuring a $[\text{PAH}]^+$ intercalated anionic inorganic layer of $[\text{In}_3\text{Sb}_2\text{S}_9]_{n^{3n^-}}$. Its asymmetric unit contains three In^{3+} ions, two Sb^{3+} ions, nine S^{2-} ions, and three protonated *n*-propylamines (Figure 1a). All the In^{3+} ions are tetrahedrally coordinated by four S^{2-} ions, where the $\text{In}-\text{S}$ bond lengths range from 2.417(4) to 2.486(4) Å. Both Sb^{3+} ions adopt slightly distorted $\{\text{SbS}_3\}$ trigonal pyramidal coordination geometries with $\text{Sb}-\text{S}$ bond lengths lying in the range of 2.401(4)–2.430(4) Å. The $[\text{In}_3\text{Sb}_2\text{S}_9]_{n^{3n^-}}$ layer can be viewed as the alternating linkages of the $\{\text{In}_2\text{Sb}_2\text{S}_8\}_n$ ribbon and the $\{\text{In}_4\text{Sb}_2\text{S}_{12}\}_n$ double-ribbon (Figure 1b). In the former ribbon, the alternating connection of two $\{\text{In}_3\text{S}_4\}$ tetrahedra and two $\{\text{Sb}_2\text{S}_3\}$ trigonal pyramids gives rise to a tetranuclear heterometallic $\{\text{In}_2\text{Sb}_2\text{S}_{10}\}$ cluster, which further connects with the neighboring ones by edge-sharing ($\text{In}3-\text{S}7-\text{Sb}2$). Such an $\{\text{In}_2\text{Sb}_2\text{S}_8\}_n$ ribbon has only been reported in $[(\text{Me})_2\text{NH}_2]_2[\text{In}_2\text{Sb}_2\text{S}_7]$,⁴³ $[(\text{Co}(\text{en}))_3]_3(\text{en})[\text{In}_6\text{Sb}_6\text{S}_{21}] \cdot \text{H}_2\text{O}$,⁵¹ and $[(\text{Ni}(\text{en}))_3]_3(\text{en})[\text{In}_6\text{Sb}_6\text{S}_{21}]$.⁵² On the other hand, in the $\{\text{In}_4\text{Sb}_2\text{S}_{12}\}_n$ double-ribbon, one $\{\text{Sb}_1\text{S}_3\}$, one $\{\text{In}1\text{S}_4\}$, and one $\{\text{In}2\text{S}_4\}$ are interconnected by corner-sharing to form a $\{\text{In}_2\text{Sb}_8\}$ cluster containing 3-membered ring (3-MR) of $\{\text{In}_2\text{Sb}_3\}$. This $\{\text{In}_2\text{Sb}_8\}$ cluster also occurred in early reported $[\text{Ni}(\text{dien})_2]_3(\text{In}_3\text{Sb}_2\text{S}_9)_2 \cdot 2\text{H}_2\text{O}$,⁵³ $[(\text{CH}_3\text{CH}_2\text{CH}_2)_2\text{NH}_2]_5\text{In}_5\text{Sb}_6\text{S}_{19} \cdot 1.45\text{H}_2\text{O}$,⁵⁴ and $[\text{Ni}(\text{en})_3] \cdot [\text{InSb}_4]$.⁵⁵ The $\{\text{In}_2\text{Sb}_8\}$ clusters arrange along the *b* axis and share the $\text{S}3$ ions to generate an infinite $\{\text{In}_2\text{Sb}_7\}_n$ ribbon. A pair of such ribbons further merges into a double-ribbon of $\{\text{In}_4\text{Sb}_2\text{S}_{12}\}_n$ by sharing the common $\text{S}4$ ions. Simultaneously, 5-MR of $\{\text{In}_3\text{Sb}_2\text{S}_5\}$ can be observed in this double-ribbon, and they interconnect with each other in a zigzag fashion along the *b* axis by sharing the $\text{In}1-\text{S}4-\text{Sb}1$ edges. To the best of our knowledge, this type of double-ribbon was never reported in the M–Sb–Q compounds. Ultimately, the $\{\text{In}_4\text{Sb}_2\text{S}_{12}\}_n$ double-ribbon and $\{\text{In}_2\text{Sb}_2\text{S}_8\}_n$ ribbon arrange alternately in *ABA'B'* sequence and interconnect via $\text{S}6$ ions, leading to the formation of an anionic $[\text{In}_3\text{Sb}_2\text{S}_9]_{n^{3n^-}}$ layer (Figure 1b). Besides the 3-MR and 5-MR mentioned above, two other ringlike windows accompanied the formation of the layer, namely, the 4-MR of $\{\text{In}_2\text{Sb}_2\text{S}_4\}$ and 6-MR of $\{\text{In}_5\text{Sb}_6\}$ (Figure 1c). Although having the same stoichiometry ($\text{In}:\text{Sb}:\text{S} = 3:2:9$), the structural feature of the inorganic layer of **1** differs entirely from that of the recently reported $[\text{Ni}(\text{dien})_2]_3(\text{In}_3\text{Sb}_2\text{S}_9)_2 \cdot 2\text{H}_2\text{O}$.⁵³ The former one is built up by the combination of two distinct subunits of ribbon, while the latter one contains large 12-MRs constructed by $\{\text{In}_3\text{S}_4\}$ tetrahedra and $\{\text{Sb}_2\text{S}_3\}$ trigonal pyramids (Figure S2 in the Supporting Information).

Actually, the $[\text{In}_3\text{Sb}_2\text{S}_9]_{n^{3n^-}}$ layer of **1** can be viewed as a reassembly of the known $[\text{In}_2\text{Sb}_2\text{S}_7]_{n^{2n^-}}$ layer of $[(\text{Me})_2\text{NH}_2]_2[\text{In}_2\text{Sb}_2\text{S}_7]$ ⁴³ by incorporating the $\{\text{In}_4\text{Sb}_2\text{S}_{12}\}_n$ double-ribbons. As shown in Figure 2d, every adjacent two

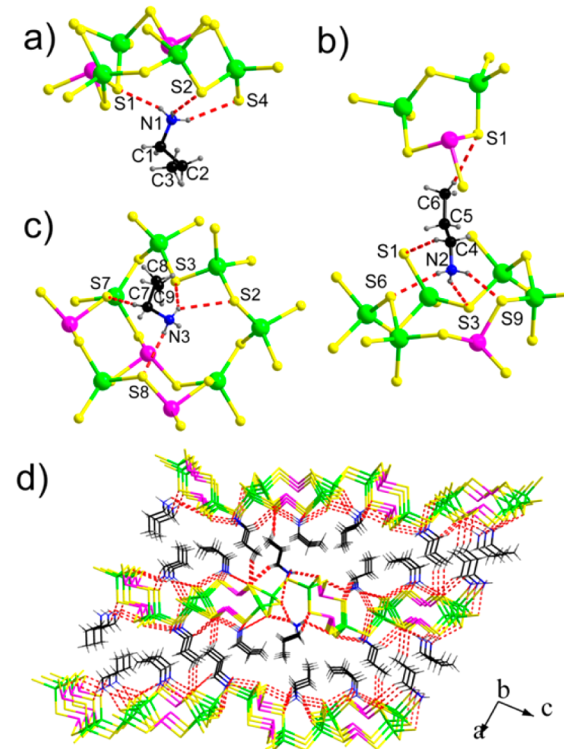


Figure 2. (a–c) Ball-and-stick representations of hydrogen bonds between the inorganic framework and the three crystallographically independent $[\text{PAH}]^+$ ions in **1**. (d) A wire/stick view of the 3D supramolecular framework of **1** along the *b* axis (dashed lines represent the $\text{N}-\text{H}\cdots\text{S}$ and $\text{C}-\text{H}\cdots\text{S}$ hydrogen bonds).

$\{\text{In}_2\text{Sb}_2\text{S}_8\}_n$ ribbons in the $[\text{In}_2\text{Sb}_2\text{S}_7]_{n^{2n^-}}$ layer share their terminal S^{2-} ions with the incoming $\{\text{In}_4\text{Sb}_2\text{S}_{12}\}_n$ double-ribbon to form the $[\text{In}_3\text{Sb}_2\text{S}_9]_{n^{3n^-}}$ layer. Because of the lower symmetry of the inserted $\{\text{In}_4\text{Sb}_2\text{S}_{12}\}_n$ double-ribbon, the original C_2 symmetrical characteristic of the $[\text{In}_2\text{Sb}_2\text{S}_7]_{n^{2n^-}}$ disappears in the newly formed $[\text{In}_3\text{Sb}_2\text{S}_9]_{n^{3n^-}}$ layer.

The $[\text{In}_3\text{Sb}_2\text{S}_9]_{n^{3n^-}}$ layers of **1** stack in an *AAA* sequence along the *a* axis. The $[\text{PAH}]^+$ ions playing structure-directing and charge-balancing roles are located in the interlayer spaces and form extensive $\text{N}-\text{H}\cdots\text{S}$ and $\text{C}-\text{H}\cdots\text{S}$ hydrogen bonds with the S^{2-} ions of the inorganic layer, Figure 2a–c. As a result, the interconnection of the $[\text{In}_3\text{Sb}_2\text{S}_9]_{n^{3n^-}}$ layers with amines via hydrogen bonds results in a 3D supramolecular framework, Figure 2d.

$[\text{Fe}(\text{en})_3]\text{In}_3\text{Sb}_2\text{S}_7$ (**2**). Compound **2** crystallizes in the monoclinic space group $P2_1/n$, featuring a layered In–Sb–S network isolated by using $[\text{Fe}(\text{en})_3]^{2+}$ as structure-directing agent (SDA) and charge-balancing agent. The asymmetric unit of **2** consists of two In^{3+} ions, two Sb^{3+} ions, seven S^{2-} ions, and one $[\text{Fe}(\text{en})_3]^{2+}$ complex, Figure 3a. The In^{3+} and Sb^{3+} ions in **2** are surrounded by four and three S^{2-} ions, respectively, forming the distorted $\{\text{InS}_4\}$ and $\{\text{SbS}_3\}$ tetrahedral coordination geometries similar to those in **1**. The bond lengths of $\text{In}-\text{S}$ and $\text{Sb}-\text{S}$ lie in the normal ranges of 2.4137(12)–2.4915(14) Å and 2.4171(14)–2.4630(14) Å, respectively. Compound **2** is relevant to the recently reported $[\text{Ni}(\text{en})_3][\text{In}_2\text{Sb}_2\text{S}_7]$,⁵² whose

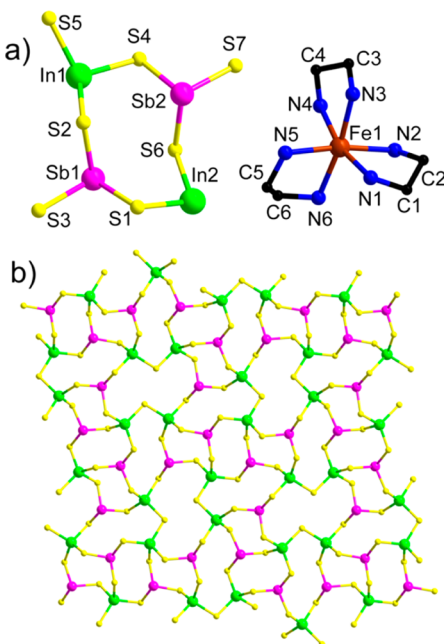


Figure 3. Ball-and-stick representations of (a) the asymmetric unit and (b) the structure of the $[In_2Sb_2S_7]_n^{2n-}$ layer of **2**.

anionic section features the identical $[In_2Sb_2S_7]_n^{2n-}$ layer, Figure 3b. Detailed structural analysis reveals that the $[In_2Sb_2S_7]_n^{2n-}$ layer is constructed by the alternating connection of $\{In_2S_7\}$ groups and $\{SbS_3\}$ trigonal pyramids through sharing vertices. In this case, each pair of adjacent Sb³⁺ ions is interlinked by two $\{In_2S_7\}$ groups as bridges. For each bridge, the two vertex S²⁻ bonded to Sb³⁺ come from either one In³⁺ (mode 1) or two In³⁺ (mode 2) of one $\{In_2S_7\}$ group. As a result, the varied combination between two different linkage modes generates three distinct ringlike windows: (a) (mode 1) \times 2 generates a 4-MR of $\{In_2Sb_2S_4\}$; (b) (mode 1) + (mode 2) generates a 5-MR of $\{In_3Sb_2S_5\}$; (c) (mode 2) \times 2 generates a 6-MR of $\{In_4Sb_2S_6\}$. The 4-MR and 5-MR are identical with those observed in compound **1**, while the 6-MR of $\{In_4Sb_2S_6\}$ adopts a distinct configuration from the 6-MR in **1** due to their different compositions as well as arrangements.

The $[In_2Sb_2S_7]_n^{2n-}$ layers of **2** stack in an AAA sequence along the *a* axis, leaving the interlayer space occupied by the charge-compensating $[Fe(en)_3]^{2+}$. Both Δ and Λ conformations of the $[Fe(en)_3]^{2+}$ are presented as a result of the centrosymmetric nature of the structure (Figure S3 in the Supporting Information). These inorganic layers are interconnected by the $[Fe(en)_3]^{2+}$ complexes to form a 3D supramolecular network through N–H···S and C–H···S hydrogen bonds (Figure 4).

$[Mg(dien)_2][In_2Sb_2S_7]\cdot 0.5H_2O$ (**3**). Compound **3** belongs to the noncentrosymmetric orthorhombic space group of *Aba*2. Its structure features an inorganic anionic 2D network built upon the In/Sb heterometallic cluster as a SBU with the metal complex cations located in the interlayer space. The asymmetric unit of **3** consists of two In³⁺ ions, two Sb³⁺ ions, half a H₂O molecule, one $[Mg(dien)_2]^{2+}$ complex, six S²⁻ ions (S1, S2, S4, S5, S6, and S7) and other two half of S²⁻ ions with C₂ symmetry (S3 and S8, 4*a* site) (Figure 5a). Both In³⁺ ions are tetrahedrally coordinated by four S²⁻ ions. Both Sb³⁺ ions adopt a {SbS₃} trigonal pyramidal coordination geometry, with Sb–S

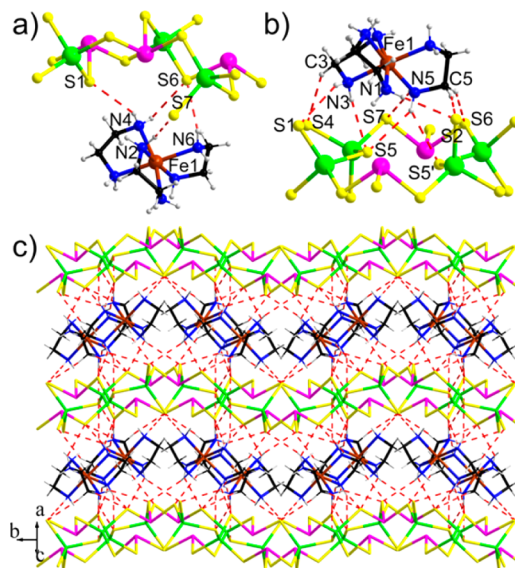


Figure 4. (a, b) Ball-and-stick representations of hydrogen bonds between the $[In_2Sb_2S_7]_n^{2n-}$ layer and the $[Fe(en)]^{2+}$ complex in **2**. (c) A wire/stick view of the 3D supramolecular framework of **2** (dashed lines represent the N–H···S and C–H···S hydrogen bonds).

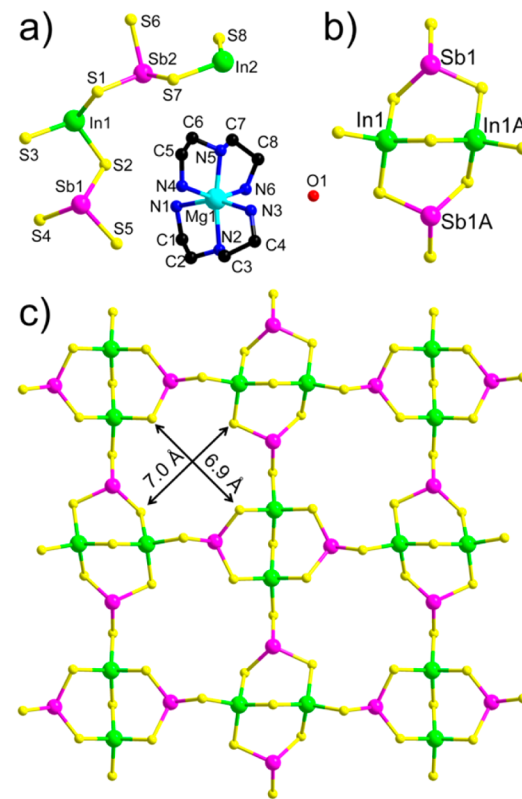


Figure 5. Ball-and-stick representations of (a) the asymmetric unit, (b) the $\{In_2Sb_2S_9\}$ cluster, and (c) the structure of the $[In_2Sb_2S_7]_n^{2n-}$ layer of **3**. Symmetry codes: A (1 – *x*, –*y*, *z*).

bond lengths ranging from 2.407 to 2.414 Å. Two $\{InS_4\}$ and two $\{Sb1S_3\}$, or two $\{In2S_4\}$ and two $\{Sb2S_3\}$ are alternately connected by corner-sharing to form a $\{In_2Sb_2S_9\}$ heterometallic cluster as the SBU, Figure 5b. Each $\{In_2Sb_2S_9\}$ cluster is connected with adjacent four clusters through the terminal S1 and S5 ions, leading to a 2D anionic network of $[In_2Sb_2S_7]_n^{2n-}$ along the *ab* plane, Figure 5c. The windows perforated on the

$[\text{In}_2\text{Sb}_2\text{S}_7]_{n^{2n^-}}$ layer are defined by the large rectangular 8-MRs of $\{\text{In}_4\text{Sb}_4\text{S}_8\}$ among the SBUs, with dimensions of $6.9 \times 7.0 \text{ \AA}$ (the short and long axes of the window, excluding van der Waals radii).

For chalcogenidometalates, hitherto, still limited progress has been made on the exploitation of SBUs integrating both tetrahedron and other polyhedron, especially those with asymmetric coordination geometries. The $\{\text{In}_2\text{Sb}_2\text{S}_9\}$ clusters in **3** resemble the earlier reported $\{\text{Ga}_2\text{Sb}_2\text{S}_9\}$ clusters, which interlink each other to form the 2D- $[\text{Ga}_2\text{Sb}_2\text{S}_7]_{n^{2n^-}}$ network.^{48,56-58} Compared to **3**, the $\{\text{Ga}_2\text{Sb}_2\text{S}_9\}$ clusters in the $[\text{Ga}_2\text{Sb}_2\text{S}_7]_{n^{2n^-}}$ layer adopt a similar arrangement but a slightly different orientation owing to a more distorted configuration of the $\{\text{Ga}_2\text{Sb}_2\text{S}_9\}$ heterometallic cluster. Such a framework flexibility was wonderfully evidenced by the dynamic response of $[\text{Ga}_2\text{Sb}_2\text{S}_7]_{n^{2n^-}}$ layer to Cs^+ insertion.⁵⁶ The $\{\text{In}_2\text{Sb}_2\text{S}_9\}$ cluster was also observed in the aforementioned 3D open framework of $[\text{In}_6\text{Sb}_6\text{S}_{21}]_{n^{6n^-}}$ as a connection point to combine $\{\text{In}_2\text{Sb}_2\text{S}_8\}$ chains.^{51,52} However, the interconnection between $\{\text{In}_2\text{Sb}_2\text{S}_9\}$ clusters themselves was not documented yet until the present example of compound **3**.

The $[\text{In}_2\text{Sb}_2\text{S}_7]_{n^{2n^-}}$ layers of **3** stack in an *ABAB* sequence along the *c* axis. The counter cations between the adjacent layers are two optically active isomers of magnesium complex, namely, the *mer*-($\delta\lambda\delta\lambda$)- $[\text{Mg}(\text{dien})_2]^{2+}$ and *mer*-($\lambda\delta\lambda\delta$)- $[\text{Mg}(\text{dien})_2]^{2+}$ (Figure S4 in the Supporting Information). As far as we know, the alkaline earth metal–amine complexes were seldom documented for being used as SDAs in the formation of thioindates or thioantimonates.^{59,60} In compound **3**, $[\text{Mg}(\text{dien})_2]^{2+}$ complexes play the structure-directing role together with extra H_2O molecules and balance the negative charge of the anionic layers. These complexes interconnect with the layers into a 3D supramolecule through extensive N–H…S, N–H…O, and C–H…S hydrogen bonds, Figure 6.

Notably, the inorganic layer of our earlier reported $[(\text{Me}_2\text{NH}_2)_2][\text{In}_2\text{Sb}_2\text{S}_7]$ ⁴³ as well as those in compounds **2** and **3** possesses an exactly identical composition of In:Sb:S = 2:2:7, motivating us to compare them in detail from a structural viewpoint. For clarity, here, we abbreviate these three types of layers in $[(\text{Me}_2\text{NH}_2)_2][\text{In}_2\text{Sb}_2\text{S}_7]$, **2**, and **3** as $\text{In}_2\text{Sb}_2\text{S}_7\text{-I}$, $\text{In}_2\text{Sb}_2\text{S}_7\text{-II}$, and $\text{In}_2\text{Sb}_2\text{S}_7\text{-III}$, respectively. Although three layers are all constructed by the dimeric $\{\text{In}_2\text{S}_7\}$ groups and discrete three-coordinated Sb^{3+} ions, the diversified configurations of the $\{\text{In}_2\text{S}_7\}$ and different linkage modes between adjacent Sb^{3+} make cases complicated, Figure 7. (a) The $\{\text{In}_2\text{S}_7\}$ groups in $\text{In}_2\text{Sb}_2\text{S}_7\text{-I}$ and $\text{In}_2\text{Sb}_2\text{S}_7\text{-III}$ are constructed in a regular fashion with C_2 symmetry, where there is a 2-fold axis that goes through the corner-shared S^{2-} ion. On the contrary, the $\{\text{In}_2\text{S}_7\}$ group in $\text{In}_2\text{Sb}_2\text{S}_7\text{-II}$ comes into being with a slight distortion, which loses the C_2 symmetry itself. This is consistent with the characteristics of the space groups they belong to, namely, $C2/c$ for $[(\text{Me}_2\text{NH}_2)_2][\text{In}_2\text{Sb}_2\text{S}_7]$, $Aba2$ for **3**, and $P2_1/n$ for compound **2**. (b) As mentioned earlier in the description of $\text{In}_2\text{Sb}_2\text{S}_7\text{-II}$ in **2**, each pair of adjacent Sb^{3+} ions are interlinked by two $\{\text{In}_2\text{S}_7\}$ groups in three different means. Although each two adjacent Sb^{3+} ions in $\text{In}_2\text{Sb}_2\text{S}_7\text{-I}$ are also connected through two $\{\text{In}_2\text{S}_7\}$ groups, however, there are only two combinations between them, namely, (mode 1) $\times 2$ and (mode 2) $\times 2$. In comparison, the case for $\text{In}_2\text{Sb}_2\text{S}_7\text{-III}$ is more different. On the one hand, two adjacent Sb^{3+} ions in the large $\{\text{In}_4\text{Sb}_4\text{S}_8\}$ ring are connected by one $\{\text{In}_2\text{S}_7\}$ group through mode 1. On the other hand, the adjacent Sb^{3+} ions in the $\{\text{In}_2\text{Sb}_2\text{S}_9\}$ unit adopt a third linkage mode by using two In^{3+}

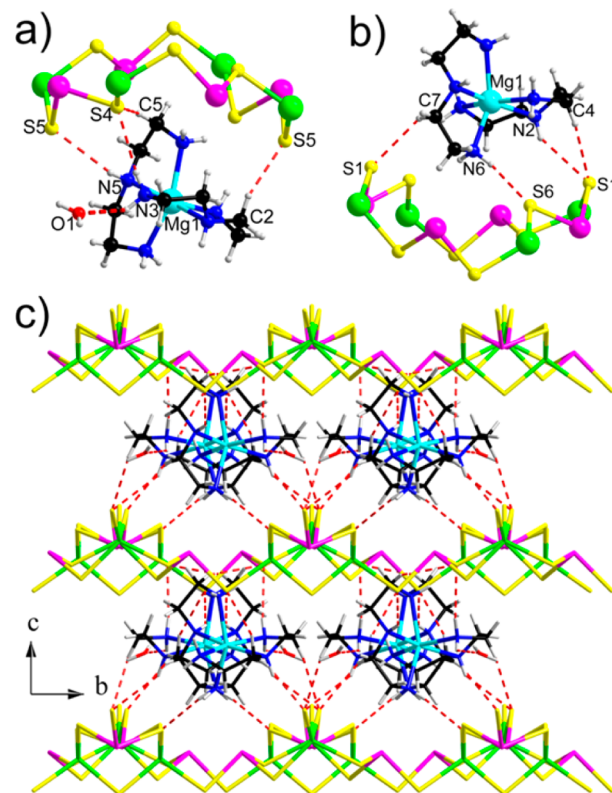


Figure 6. (a, b) Ball-and-stick representations of hydrogen bonds between the $[\text{In}_2\text{Sb}_2\text{S}_7]_{n^{2n^-}}$ layer and the $[\text{Fe}(\text{en})_3]^{2+}$ complex in **3**. (c) A wire/stick view of the 3D supramolecular framework of **3** along the *a* axis (dashed lines represent the N–H…S, N–H…O, and C–H…S hydrogen bonds).

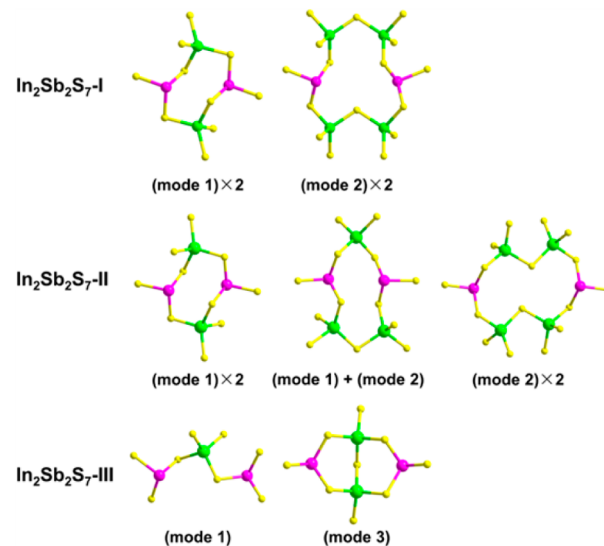


Figure 7. Different combinations of linkage modes between two adjacent Sb^{3+} ions in $\text{In}_2\text{Sb}_2\text{S}_7\text{-I}$, $\text{In}_2\text{Sb}_2\text{S}_7\text{-II}$, and $\text{In}_2\text{Sb}_2\text{S}_7\text{-III}$.

ions of one $\{\text{In}_2\text{S}_7\}$ group as two bridges (mode 3). Anyway, the formation of a certain type of structure of the inorganic framework will be clearly influenced by its corresponding SDAs with various sizes, shapes, and charges, such as the $[(\text{Me}_2\text{NH}_2)_2]^+$, $[\text{Ni}(\text{en})_3]^{2+}$, and $[\text{Mg}(\text{dien})_2]^{2+}$ in the above three compounds.

$\text{In}_2(\text{N,N-dmen})_2\text{Sb}_2\text{S}_6$ (**4**). Compared to the 1D, 2D, or 3D structures of the inorganic segments, the discrete cluster was rarely reported in the 13/15/16 group family, to the best of our knowledge, only evidenced by the cationic $\{[\text{In}(\text{C}_6\text{H}_{14}\text{N}_2)_2]_2\text{Sb}_4\text{S}_8\}^{2+}$ recently isolated by Bensch's group.⁶¹ However, a neutral discrete In–Sb–S cluster in this family has never been discovered until our present work. Compound **4** features a novel neutral $\{\text{In}_2(\text{N,N-dmen})_2\text{Sb}_2\text{S}_6\}$ cluster, representing the first example of inorganic–organic hybrid molecule in the 13/15/16 family. It crystallizes in the monoclinic space group $P2_1/c$. The asymmetric unit of compound **4** contains one In^{3+} , one Sb^{3+} , three S^{2-} , and one N,N-dmen ligand. The Sb^{3+} ion is surrounded by three S^{2-} ions, adopting a typical trigonal pyramidal coordination geometry, where the Sb–S bonds are in the common range of $2.399(2)$ – $2.4366(19)$ Å. Notably, the In^{3+} ion is octahedrally bonded by four S^{2-} ions and two N atoms of the N,N-dmen in *cis*-conformation, representing a rare six-coordination mode in the chalcogenidoindates. The average value of four In–S bond lengths ($2.6172(19)$ Å) in **4** is longer than the normal In–S bond lengths of the $\{\text{InS}_4\}$ tetrahedron (~ 2.4 – 2.5 Å), which is in accordance with the steric effect around the In^{3+} ion. Bond valence summary (BVS) value of $s = 2.912$ affirmed the +3 oxidation state of the In^{3+} ion.⁶² The structure of the molecular $\{\text{In}_2(\text{N,N-dmen})_2\text{Sb}_2\text{S}_6\}$ cluster is shown in Figure 8a. A pair of

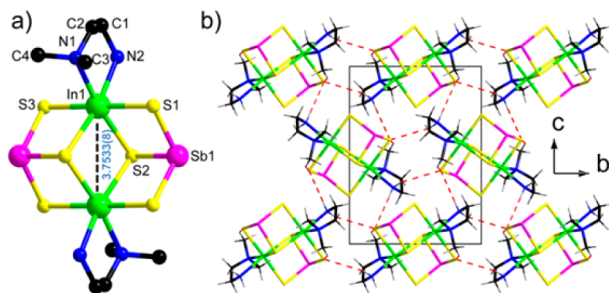


Figure 8. (a) The $\{\text{In}_2(\text{N,N-dmen})_2\text{Sb}_2\text{S}_6\}$ cluster in **4**. (b) A wire/stick view of the 3D supramolecular framework of **4** along the a axis (dashed lines represent the N–H···S and C–H···S hydrogen bonds).

centrosymmetrically related $\{\text{SbS}_3\}$ groups are bridged by two $[\text{In}(\text{N,N-dmen})]^{2+}$ through sharing the $\mu_2\text{-S}$ ions ($\text{S}1$ and $\text{S}3$) and $\mu_3\text{-S}$ ion ($\text{S}2$), resulting in an organic-decorated double-semicubane-like $\{\text{In}_2(\text{N,N-dmen})_2\text{Sb}_2\text{S}_6\}$ cluster, with the In^{3+} – In^{3+} distance of $3.7533(8)$ Å, Figure 8a. The architecture of such a cluster resembles the familiar anionic $\{\text{Mn}_2(\text{phen})_2\text{As}^{\text{III}}\text{S}_6\}$ or $\{\text{Mn}_2(\text{phen})_2\text{Sb}^{\text{III}}\text{S}_6\}$ clusters that are connected by $[\text{Mn}_2(\text{phen})]^{2+}$ or Hg^{2+} to form infinite chainlike structures.^{63,64} Nevertheless, the discrete, neutral $\{\text{In}_2(\text{N,N-dmen})_2\text{Sb}_2\text{S}_6\}$ cluster differs from the two 1D species mentioned above owing to the higher oxidation state of In^{3+} compared to Mn^{2+} , which completely balance the negative charge of the two $\{\text{SbS}_3\}$ groups. The N,N-dmen ligand chelates to the In^{3+} ion through two In–N coordination bonds. It illustrates the feasibility of constructing a high dimensional inorganic–organic hybrid by the combination of the inorganic node of $\{\text{In}_2\text{Sb}_2\text{S}_6\}$ and suitable multidentate ligand, analogous to the cases in some Mn–Sb–S compounds. Extensive intermolecular N–H···S and C–H···S hydrogen bonds connect the $\{\text{In}_2(\text{N,N-dmen})_2\text{Sb}_2\text{S}_6\}$ clusters into a 3D supramolecular network, Figure 8b.

In–Sb–S Architectures Containing Organic Amines. Hitherto, the progress made in the study on the M–Sb–Q (M = Ga, In, Ge, Sn; Q = S, Se) compounds containing organic amines drives us to exploit the characteristics and roles of these organic species in the crystalline products. The purpose is to supply powerful information for designing new compounds with certain structural features and predicting the possible functions behind them. It is a great challenge owing to not only the limited number of examples reported up to now but also the varied SDAs with size and shape versatility. As a relatively better-established area, the syntheses, structures, and characterizations of the organic amine-containing In–Sb–S compounds have attracted attention from several research groups, e.g., Kanatzidis' group, Huang's group, Zhou's group, etc. All these above-mentioned structures are summarized in Figure 9.⁶⁵ Herein, we will talk in a primary step about the influence of organic amines on the structures of In–Sb–S compounds.

The discussion starts with the primary and secondary amines. These two types of amines have the same charge of +1 while they vary in parameters such as shape and size, resulting in different structures of the inorganic networks shown in the first row of Figure 9. (a) The $[\text{In}_4\text{Sb}_9\text{SH}]_n^{4n-}$ directed by $[\text{NH}_3\text{CH}_3]^+$ is the only 3D-framework among them,⁴⁴ whose structure is similar to that of the $[\text{NH}_4]^+$ -directed 3D- $[\text{Ga}_4\text{Sb}_9\text{S}_1]_n^{5n-}$ framework.⁶⁶ Such a structural similarity is reasonable because $[\text{NH}_3\text{CH}_3]^+$ is a rigid amine with a relatively larger size than that of $[\text{NH}_4]^+$, which matches better to the larger pores of the $[\text{In}_4\text{Sb}_9\text{SH}]_n^{4n-}$ framework ($r \sim 1.72$ – 1.93 Å) compared with those of $[\text{Ga}_4\text{Sb}_9\text{S}_1]_n^{5n-}$ ($r \sim 1.67$ – 1.77 Å). (b) As for other amines with longer alkyl groups, they have more softness and flexibility caused by the free rotation of the group along the C–C or C–N bonds.⁶ These characteristics probably make the amines easier to arrange in the interspace of 2D networks, in good agreement with the diversified distances and flexible slip between two adjacent layers. (c) Although having the same size and conformation, the secondary amine $[(\text{Me})_2\text{NH}_2]^+$ can combine well with the $[\text{In}_2\text{Sb}_2\text{S}_7]^{2-}$ layer ($\text{In}_2\text{Sb}_2\text{S}_7\text{-I}$), while the primary amine, namely, the $[\text{NH}_3\text{CH}_2\text{CH}_3]^+$, has not been documented as SDA in any inorganic In–Sb–Q network yet, to the best of our knowledge. Actually, the protonated amines have surfactant-like behavior, where the hydrophilic group (containing N atom) has a higher tendency to facing the anionic network while the hydrophobic group (carbon skeleton) likes pointing toward the void around the framework.^{67,68} So the position of the N atom in the organic amine may somehow affect the fitness between the SDA and inorganic host.

The chelating polyamines, on the other hand, initially display a tendency to coordinate to metal ions to form metal complexes. These *in situ* formed complexes not only play a charge-balancing role but, more importantly, can act as SDAs with different characteristics compared to the organic amines. (a) The metal complexes possess relatively larger dimensions, which contribute to the presence of larger cavities in the corresponding inorganic frameworks. This can be directly evidenced by the presence of open windows as large as 20- and 16-MR in the 3D- $[\text{In}_6\text{Sb}_6\text{S}_{21}]_n^{6n-51,52}$ and 3D- $[\text{InSb}_3\text{S}_7]_{2n}^{69}$ frameworks directed by transition metal complexes (TMCs), respectively. (b) The conformations of metal complexes exhibit a great variety. For those with three bidentate ligands, i.e., $[\text{M}(\text{en})_3]^{2+}$, the absence of the symmetry plane and inversion center leads to its adoption of two possible optical forms, either Δ or Λ . Besides, the organic ligands can also contribute to the

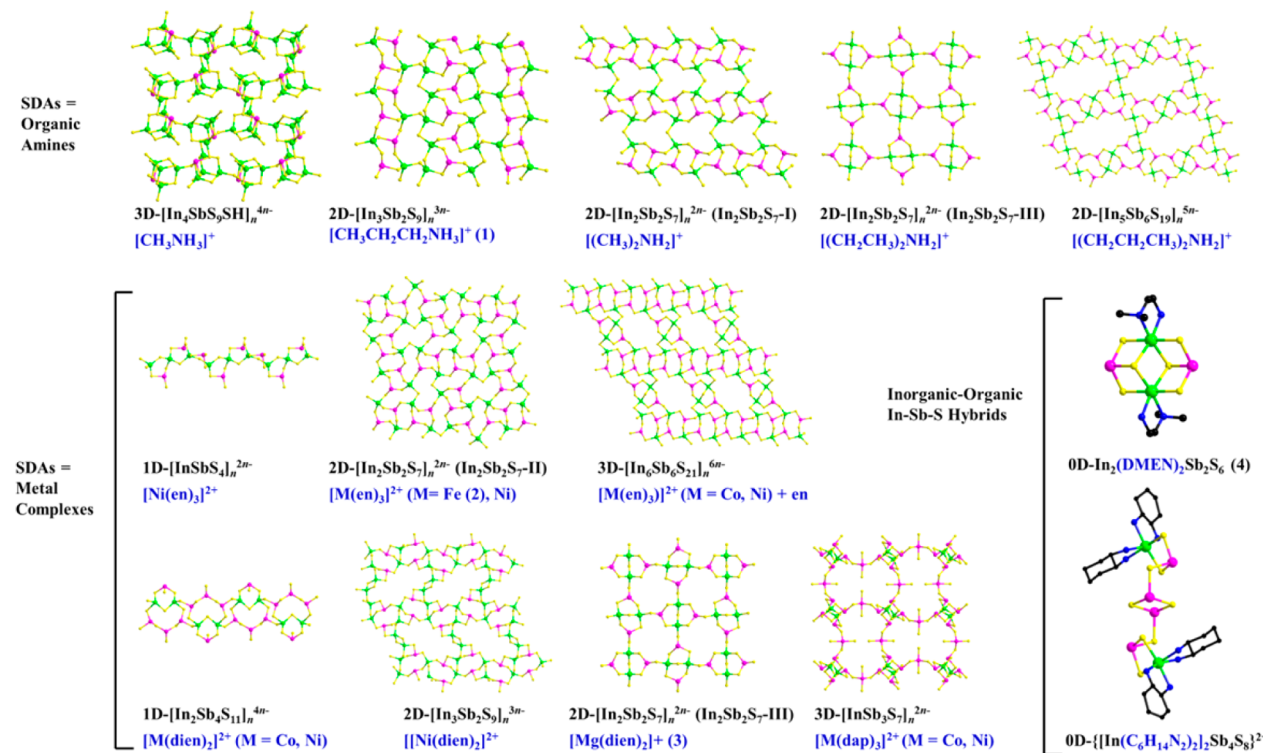


Figure 9. Variation of the inorganic In–Sb–Q segments (written in black) and their corresponding organic SDAs (written in blue).

asymmetry when they bond to the coordination center, forming δ or λ modes. Such asymmetric characteristics can sometimes introduce polar feature into the inorganic segments, evidenced by the chiral 1D-[InSbS₄]_n²ⁿ⁻ chain directed by Λ -[Ni(en)]₃²⁺ complexes,⁵⁵ while in many cases, two enantiomers of the metal complexes are presented together due to the centrosymmetric nature of the structure, which occurs not only in the In–Sb–S family^{51,52} but also in others.^{70,71} In comparison, cases become more complicated for the metal complexes constructed by tridentate ligands. Taking the dien for example, different ways of arranging the N donor atoms in the ideal [MA₃B₃] model lead to three geometrical isomers, namely the optically active *u-fac* and *mer* isomers and the optically inactive *s-fac* isomer. By now, all three isomers have been observed in the In–Sb–S family, such as the *u-fac*- and *mer*-[Ni(dien)]₂²⁺ in the [Ni(dien)]₂₃[In₃Sb₂S₉]₂·2H₂O⁵³ and *s-fac*- and *u-fac*-[M(dien)]₂²⁺ in [M(dien)]₂₂[In₂Sb₄S₁₁] (M = Co, Ni).^{53,72} (c) Same or similar metal complex system reveals diversification of its directing role. For instance, with the presence of both Ni²⁺ and en, the resulting inorganic segments exhibit three types, including 1D-[InSbS₄]_n²ⁿ⁻,⁵⁵ 2D-[In₂Sb₂S₇]_n²ⁿ⁻,⁵² and 3D-[In₆Sb₆S₂₁]_n⁶ⁿ⁻.^{51,52} For the 1D-[InSbS₄]_n²ⁿ⁻, as mentioned earlier, the presence of Λ -[Ni(en)]₃²⁺ complex alone and the chiral feature of the inorganic chain implies the transfer of polarity between them. By contrast, the 2D-[In₂Sb₂S₇]_n²ⁿ⁻ exhibit a centrosymmetric feature, which is consistent with the coexistence of Δ - and Λ -[Ni(en)]₃²⁺ in the structure. However, although the Δ - and Λ -[Ni(en)]₃²⁺ are also present in the compound [(Ni(en))₃]₃(en)[In₆Sb₆S₂₁], the inorganic 3D-[In₆Sb₆S₂₁]_n⁶ⁿ⁻ turns out to be another structural feature different from that of 2D-[In₂Sb₂S₇]_n²ⁿ⁻, which could be related to the cocrystallized en molecule as an auxiliary templating agent. In addition to the above example, a similar situation also occurs between the 1D-[In₂Sb₄S₁₁]_n⁴ⁿ⁻ and 2D-[In₃Sb₂S₉]_n³ⁿ⁻, which are both directed by the [Ni(dien)]₂²⁺ complex.⁵³ This

mechanism for structural diversification is still poorly understood, while it should be strongly related to the variable interplay of a wide range of reaction parameters, including the nature and molar ratio of initial reactants, reaction time, solvent, pressure, temperature and pH value, etc.

In the third situation, the amines can interact directly with the inorganic segments through coordination bonds, resulting in the rare inorganic–organic hybrid compounds with low dimensional architectures, Figure 9. Such a binding mode is somehow similar to the cases occurred in the {TM(L)_n}–As–Q and {TM(L)_n}–Sb–Q families, where the {TM(L)_n} means unsaturated metal complexes with capacity to further interact with the inorganic segments via covalent M–Q bonds.^{73,74} In the case of {[In(C₆H₁₄N₂)₂]Sb₄S₈}²⁺,⁶¹ for example, the central [Sb₄S₈]⁴⁻ anion exhibits the same composition whereas a different bonding pattern compared to that observed in [TM(tren)]₂[Sb₄S₈] (TM = Co, Zn; tren = tris(2-aminoethyl)-amine).^{22,27} Here, the [In(C₆H₁₄N₂)₂]³⁺ plays a similar bonding role as the [TM(tren)]²⁺, preventing the further propagation of the inorganic [Sb₄S₈]⁴⁻ anions. Furthermore, the replacement of the TM²⁺ by In³⁺ results in a cationic feature of the formed {[In(C₆H₁₄N₂)₂]Sb₄S₈}²⁺ cluster. In comparison, the architecture of In₂(N,N-dmen)₂Sb₂S₆ (4) represents a relatively new fashion, where two bidentate N,N-dmen ligands interact with a neutral {In₂Sb₂S₆} cluster, functionalizing as an organic decorating agent. Actually, through the structural analysis, we can tell the differences between the organic ligand bonded to inorganic segment and the protonated amine or metal complex. The former features a neutral valence state and connects to the inorganic segment via strong coordination bonds. By contrast, as discrete species, the latter two act as space fillers as well as charge-balancing agents to interact with the anionic framework based on the electric forces together with hydrogen bonds. To sum up, although the coordination bond interaction between the amines and inorganic segments is

rarely observed in the 13/15/16 and 14/15/16 group compounds, the convincing feasibility demonstrated by the existing examples provides a large room to further exploit specific inorganic–organic hybrid materials exhibiting novel structure–function features.

Powder X-ray Diffraction Analyses and Optical Properties. The powder X-ray diffraction (PXRD) patterns of **1–4** are shown in Figure 10. The 2θ values for all peaks

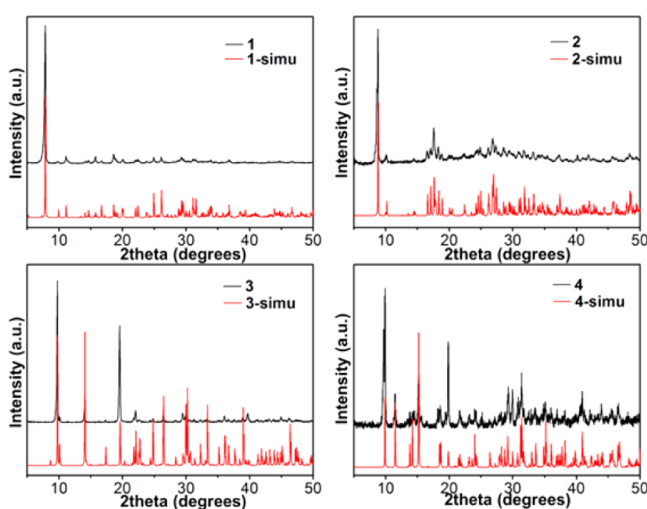


Figure 10. Experimental and simulated PXRD patterns of **1–4**.

exhibit a good match with the corresponding simulated results from the single-crystal diffraction data, indicating the high purity for all as-mentioned samples. In comparison, the intensities of several peaks do not fit very well with the simulated values owing to the preferred crystallographic orientations of the polycrystalline samples, especially for **3** and **4**. Solid-state absorption spectra of **1–4** are plotted in Figure 11. We calculated the band gap of **1–4** to be 2.99, 2.97,

the variety of the band gaps is probably due to the structural and compositional difference.

CONCLUSION

In summary, we have discussed in depth the solvothermal syntheses, structures, and characterizations of a series of novel In–Sb–S compounds containing organic amines, $[PAH]_3[In_3Sb_2S_9]$ (**1**), $[Fe(en)_3][In_2Sb_2S_7]$ (**2**), $[Mg(dien)_2][In_2Sb_2S_7] \cdot 0.5H_2O$ (**3**), and $In_2(N,N-dmen)_2Sb_2S_6$ (**4**). Compounds **1**, **2**, and **3** possess 2D anionic networks with distinct structural features, while compound **4** is composed of discrete inorganic–organic hybrid molecules. Notably, as demonstrated by the structural analyses on **1–4**, the organic amines applied here played three different roles on the formation of the final crystalline products. For **1**, the protonated amines arrange in the space around the anionic network and balance the negative charge. For **2** and **3**, the chelating polyamines coordinated to central metal ions to form metal complexes, which then act as space-filling and charge-balancing agents. In comparison, the amines in **4** interconnect with the inorganic segments through coordination bonds, leading to the formation of the rare inorganic–organic hybrid clusters. Furthermore, a systematic discussion about the characteristics and roles of these organic amines on the crystalline products was presented based on the summary of all In–Sb–S compounds documented to date. In short, the work presented here enriches the structural chemistry of the main-group heterometallic chalcogenidometalates, providing more chances for researchers to work out the rules in the composition– or structure–function relationship.

ASSOCIATED CONTENT

S Supporting Information

Additional crystallographic data for compounds **1–4** in CIF format, more structural details, EDS data, and TG data. This material is available free of charge via the Internet at <http://pubs.acs.org>. Also available from the CCDC: 888648 for **1**, 1030458 for **2**, 1030459 for **3**, 1030460 for **4**.

AUTHOR INFORMATION

Corresponding Author

*E-mail: xyhuang@fjirs.ac.cn. Fax: +86 591 83793727.

Notes

The authors declare no competing financial interest.

ACKNOWLEDGMENTS

This work was supported by grants from the NNSF of China (No. 21221001 and 21171164) and the 973 program (No. 2014CB845603).

REFERENCES

- (1) Bedard, R. L.; Wilson, S. T.; Vail, L. D.; Bennett, J. M.; Flanigan, E. M. *Stud. Surf. Sci. Catal.* **1989**, *49*, 375–387.
- (2) Li, H.; Laine, A.; O’Keeffe, M.; Yaghi, O. M. *Science* **1999**, *283*, 1145–1147.
- (3) Zheng, N.; Bu, X.; Wang, B.; Feng, P. *Science* **2002**, *298*, 2366–2369.
- (4) Zheng, N. F.; Bu, X. H.; Feng, P. Y. *Nature* **2003**, *426*, 428–432.
- (5) Li, J.; Chen, Z.; Wang, R.-J.; Proserpio, D. M. *Coord. Chem. Rev.* **1999**, *190–192*, 707–735.
- (6) Zhou, J.; Dai, J.; Bian, G.-Q.; Li, C.-Y. *Coord. Chem. Rev.* **2009**, *293*, 1221–1247.
- (7) Schur, M.; Rijnberk, H.; Näther, C.; Bensch, W. *Polyhedron* **1999**, *18*, 101–107.

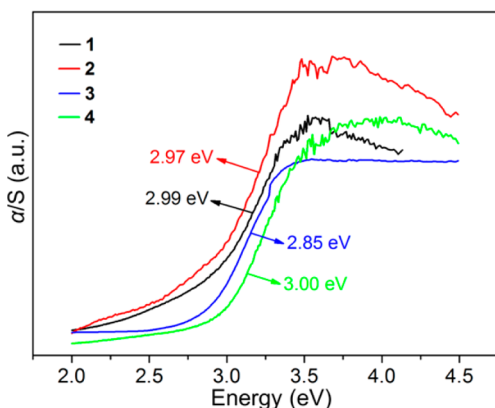


Figure 11. Solid-state UV–vis absorption spectra of compounds **1–4**.

2.85, and 3.00 eV, respectively, showing a blue shift compared with that of In_2S_3 (2.3 eV)⁷⁵ and Sb_2S_3 (1.6 eV).⁷⁶ These four values are wider than those of $[(CH_3CH_2CH_2)_2NH_2]_3In_3Sb_6S_{19} \cdot 1.45H_2O$ (2.62 eV)⁵⁴ and $[(Me)_2NH_2]_2[In_2Sb_2S_7]$ (2.31 eV),⁴³ while close to those of $[NH_3CH_3]_4[In_4Sb_9SH]$ (3.06 eV),⁴⁴ $[Ni(en)_3][InSb_4]$ (2.84 eV),⁵⁵ $[M(dap)_3]InSb_3S_7$ ($M = Co$ (3.02 eV), Ni (2.97 eV)),⁶⁹ and $[Ni(dien)_2]_3[In_3Sb_2S_9]_2 \cdot 2H_2O$ (3.04 eV),⁵³ indicating that

- (8) Vaqueiro, P.; Chippindale, A. M.; Powell, A. V. *Polyhedron* **2003**, *22*, 2839–2845.
- (9) Möller, K.; Näther, C.; Bannwarth, A.; Bensch, W. *Z. Anorg. Allg. Chem.* **2007**, *633*, 2635–2640.
- (10) Powell, A. V.; Lees, R. J. E.; Chippindale, A. M. *J. Phys. Chem. Solids* **2008**, *69*, 1000–1006.
- (11) Bensch, W.; Näther, C.; Schur, M. *Chem. Commun.* **1997**, 1773–1774.
- (12) Schaefer, M.; Näther, C.; Lehnert, N.; Bensch, W. *Inorg. Chem.* **2004**, *43*, 2914–2921.
- (13) Schaefer, M.; Kurowski, D.; Pfitzner, A.; Näther, C.; Rejai, Z.; Möller, K.; Ziegler, N.; Bensch, W. *Inorg. Chem.* **2006**, *45*, 3726–3731.
- (14) Wang, X.; Sheng, T.-L.; Hu, S.-M.; Fu, R.-B.; Wu, X.-T. *Inorg. Chem. Commun.* **2009**, *12*, 399–401.
- (15) Liu, Y.; Kanhere, P. D.; Wong, L. C.; Tian, Y.; Feng, Y.; Boey, F.; Wu, T.; Chen, H.; White, T. J.; Chen, Z.; Zhang, Q. *J. Solid State Chem.* **2010**, *183*, 2644–2649.
- (16) Liu, Y.; Tian, Y.; Wei, F.; Ping, M. S. C.; Huang, C.; Boey, F.; Kloc, C.; Chen, L.; Wu, T.; Zhang, Q. *Inorg. Chem. Commun.* **2011**, *14*, 884–888.
- (17) Nie, L.; Xiong, W.-W.; Li, P.; Han, J.; Zhang, G.; Yin, S.; Zhao, Y.; Xu, R.; Zhang, Q. *J. Solid State Chem.* **2014**, *220*, 118–123.
- (18) Gao, J.; Tay, Q.; Li, P.-Z.; Xiong, W.-W.; Zhao, Y.; Chen, Z.; Zhang, Q. *Chem.—Asian J.* **2014**, *9*, 131–134.
- (19) Kiebach, R.; Bensch, W.; Hoffmann, R.-D.; Pöttgen, R. *Z. Anorg. Allg. Chem.* **2003**, *629*, 532–538.
- (20) Kiebach, R.; Warratz, R.; Näther, C.; Bensch, W. *Z. Anorg. Allg. Chem.* **2009**, *635*, 988–994.
- (21) Stephan, H.-O.; Kanatzidis, M. G. *J. Am. Chem. Soc.* **1996**, *118*, 12226–12227.
- (22) Stähler, R.; Bensch, W. *J. Chem. Soc., Dalton Trans.* **2001**, 2518–2522.
- (23) Stähler, R.; Bensch, W. *Eur. J. Inorg. Chem.* **2001**, 3073–3078.
- (24) Engelke, L.; Näther, C.; Leisner, P.; Bensch, W. *Z. Anorg. Allg. Chem.* **2008**, *634*, 2959–2965.
- (25) Lichte, J.; Lühmann, H.; Näther, C.; Bensch, W. *Z. Anorg. Allg. Chem.* **2009**, *635*, 2021–2026.
- (26) Lühmann, H.; Rejai, Z.; Möller, K.; Leisner, P.; Ordolff, M.-E.; Näther, C.; Bensch, W. *Z. Anorg. Allg. Chem.* **2008**, *634*, 1687–1695.
- (27) Schaefer, M.; Nather, C.; Bensch, W. *Monatsh. Chem.* **2004**, *135*, 461–470.
- (28) Schimek, G. L.; Kolis, J. W.; Long, G. *J. Chem. Mater.* **1997**, *9*, 2776–2785.
- (29) Chen, Z.; Dilks, R. E.; Wang, R.-J.; Lu, J. Y.; Li, J. *Chem. Mater.* **1998**, *10*, 3184–3188.
- (30) Powell, A. V.; Boissière, S.; Chippindale, A. M. *J. Chem. Soc., Dalton Trans.* **2000**, *4192*–4195.
- (31) Powell, A. V.; Paniagua, R.; Vaqueiro, P.; Chippindale, A. M. *Chem. Mater.* **2002**, *14*, 1220–1224.
- (32) Spetzler, V.; Näther, C.; Bensch, W. *Inorg. Chem.* **2005**, *44*, 5805–5812.
- (33) Zhang, M.; Sheng, T.; Wang, X.; Hu, S.; Fu, R.; Chen, J.; He, Y.; Qin, Z.; Shen, C.; Wu, X. *CrystEngComm* **2010**, *12*, 73–76.
- (34) Zhang, C.; Ji, M.; Ji, S.-H.; An, Y.-L. *Inorg. Chem.* **2014**, *53*, 4856–4860.
- (35) Schimek, G. L.; Pennington, W. T.; Wood, P. T.; Kolis, J. W. *J. Solid State Chem.* **1996**, *123*, 277–284.
- (36) Wood, P. T.; Schimek, G. L.; Kolis, J. W. *Chem. Mater.* **1996**, *8*, 721–726.
- (37) Vaqueiro, P.; Chippindale, A. M.; Cowley, A. R.; Powell, A. V. *Inorg. Chem.* **2003**, *42*, 7846–7851.
- (38) Powell, A. V.; Thun, J.; Chippindale, A. M. *J. Solid State Chem.* **2005**, *178*, 3414–3419.
- (39) Spetzler, V.; Näther, C.; Bensch, W. *J. Solid State Chem.* **2006**, *179*, 3541–3549.
- (40) Yao, H.-G.; Ji, M.; Ji, S.-H.; Zhang, R.-C.; An, Y.-L.; Ning, G.-L. *Cryst. Growth Des.* **2009**, *9*, 3821–3824.
- (41) Yao, H.-G.; Zhou, P.; Ji, S.-H.; Zhang, R.-C.; Ji, M.; An, Y.-L.; Ning, G.-L. *Inorg. Chem.* **2010**, *49*, 1186–1190.
- (42) Feng, M.-L.; Huang, X.-Y. *Chin. J. Inorg. Chem.* **2013**, *29*, 1599–1608.
- (43) Wang, K.-Y.; Feng, M.-L.; Kong, D.-N.; Liang, S.-J.; Wu, L.; Huang, X.-Y. *CrystEngComm* **2012**, *14*, 90–94.
- (44) Wang, K.-Y.; Feng, M.-L.; Li, J.-R.; Huang, X.-Y. *J. Mater. Chem. A* **2013**, *1*, 1709–1715.
- (45) Wendlandt, W. M.; Hecht, H. G. *Reflectance Spectroscopy*; Interscience: New York, 1966.
- (46) Sheldrick, G. M. *SHELXS97* and *SHELXL97*; University of Göttingen: Germany, 1997.
- (47) Feng, M.-L.; Kong, D.-N.; Xie, Z.-L.; Huang, X.-Y. *Angew. Chem., Int. Ed.* **2008**, *47*, 8623–8626.
- (48) Feng, M.-L.; Xie, Z.-L.; Huang, X.-Y. *Inorg. Chem.* **2009**, *48*, 3904–3906.
- (49) Dong, W.; Wang, X.; Li, B.; Wang, L.; Chen, B.; Li, C.; Li, X.; Zhang, T.; Shi, Z. *Dalton Trans.* **2011**, *40*, 243–248.
- (50) Shen, Q.; Xue, J.; Liu, J.; Jia, H.; Liu, X.; Xu, B. *CrystEngComm* **2013**, *15*, 1007–1014.
- (51) Zhou, J.; An, L. *CrystEngComm* **2011**, *13*, 5924–5928.
- (52) Zhou, J.; Liu, X.; An, L.; Hu, F.; Kan, Y.; Li, R.; Shen, Z. *Dalton Trans.* **2013**, *42*, 1735–1742.
- (53) Zhou, J.; Yin, X.-H.; Zhang, F. *Inorg. Chem.* **2010**, *49*, 9671–9676.
- (54) Ding, N.; Kanatzidis, M. G. *Chem. Mater.* **2007**, *19*, 3867–3869.
- (55) Feng, M.-L.; Li, P.-X.; Du, K.-Z.; Huang, X.-Y. *Eur. J. Inorg. Chem.* **2011**, 3881–3885.
- (56) Ding, N.; Kanatzidis, M. G. *Nat. Chem.* **2010**, *2*, 187–191.
- (57) Lin, Z.; Bu, X.; Feng, P. *Microporous Mesoporous Mater.* **2010**, *132*, 328–334.
- (58) Kong, D.-N.; Feng, M.-L.; Ye, D.; Huang, X.-Y. *Chin. J. Struct. Chem.* **2010**, *29*, 905–913.
- (59) Quiroga-González, E.; Näther, C.; Bensch, W. *Z. Naturforsch. B* **2009**, *64b*, 1312–1318.
- (60) Quiroga-González, E.; Kienle, L.; Näther, C.; Chakravadhanula, V. S. K.; Lühmann, H.; Bensch, W. *J. Solid State Chem.* **2010**, *183*, 2805–2812.
- (61) Quiroga-González, E.; Näther, C.; Bensch, W. *Solid State Sci.* **2010**, *12*, 1235–1241.
- (62) Brown, I. D.; Altermatt, D. *Acta Crystallogr., Sect. B: Struct. Sci.* **1985**, *41*, 244–247.
- (63) Liu, G.-N.; Guo, G.-C.; Chen, F.; Wang, S.-H.; Sun, J.; Huang, J.-S. *Inorg. Chem.* **2011**, *51*, 472–482.
- (64) Wang, K.-Y.; Zhou, L.-J.; Feng, M.-L.; Huang, X.-Y. *Dalton Trans.* **2012**, *41*, 6689–6695.
- (65) In Figure 9, the 2D-[$\text{In}_2\text{Sb}_2\text{S}_7$]_n²ⁿ⁻ directed by [(CH₂CH₃)₂NH₂]⁺ is an unpublished result, and the optimizing reaction is still in progress for the reason of the poor quality of the crystals.
- (66) Mertz, J. L.; Ding, N.; Kanatzidis, M. G. *Inorg. Chem.* **2009**, *48*, 10898–10900.
- (67) Cahill, C. L.; Gugliotta, B.; Parise, J. B. *Chem. Commun.* **1998**, 1715–1716.
- (68) Pitzschke, D.; Näther, C.; Bensch, W. *Solid State Sci.* **2002**, *4*, 1167–1171.
- (69) Zhou, J.; An, L.; Zhang, F. *Inorg. Chem.* **2011**, *50*, 415–417.
- (70) Wang, K.-Y.; Ye, D.; Zhou, L.-J.; Feng, M.-L.; Huang, X.-Y. *Dalton Trans.* **2013**, *42*, 5454–5461.
- (71) Zhou, J.; An, L.; Liu, X.; Huang, L.; Huang, X. *Dalton Trans.* **2011**, *40*, 11419–11424.
- (72) Liu, X. *Inorg. Chem. Commun.* **2011**, *14*, 437–439.
- (73) Kromm, A.; van Almsick, T.; Sheldrick, W. S. *Z. Naturforsch. B* **2010**, *65b*, 918–936.
- (74) Seidlhofer, B.; Pienack, N.; Bensch, W. *Z. Naturforsch. B* **2010**, *65b*, 937–975.
- (75) Asikainen, T.; Ritala, M.; Leskelä, M. *Appl. Surf. Sci.* **1994**, *82–83*, 122–125.
- (76) Fujita, T.; Kurita, K.; Tokiyama, K.; Oda, T. *J. Phys. Soc. Jpn.* **1987**, *56*, 3734–3739.